ISSN: 0976-9102 (ONLINE)
DOI: 10.21917/ijivp.2026.0566

A STUDY ON ABNORMALITY DETECTION AND CLASSIFICATION OF DISEASES USING DIGITAL IMAGE PROCESSING TECHNIQUES WITH A CASE STUDY ON MRI AND X-RAY IMAGES OF ANIMALS

G.G. Rajput and Sumitra M. Mudda
Department of Computer Science, Karnataka State Women's University, India

Abstract

Early and accurate diagnosis of diseases in animals is essential for improving veterinary healthcare and reducing mortality. Traditional manual interpretation of X-ray radiographs is often time-consuming and prone to human error, especially in rural veterinary practices. This research presents an automated disease detection framework using Digital Image Processing (DIP) techniques applied to animal X-ray images. The proposed methodology includes image preprocessing, segmentation, feature extraction, and classification using both classical machine learning and deep learning algorithms. Various abnormalities such as bone fractures, lung infections, and soft-tissue irregularities were analyzed. Experimental results demonstrate that deep learning models, particularly Convolutional Neural Networks (CNNs), significantly outperform conventional approaches with improved accuracy and robustness. The study concludes that digital image processing provides an efficient, scalable, and cost-effective diagnostic support system for veterinary medicine.

Keywords:

Digital Image Processing, Animal X-Ray, Disease Detection, Image Segmentation, Feature Extraction, Classification, Machine Learning, Deep Learning, Veterinary Diagnosis

1. INTRODUCTION

In veterinary medicine, fractures are a frequent occurrence, and it is often necessary to make a rapid and correct diagnosis in order to guarantee that animals get the required therapy and recover in a timely manner [1]. The poor quality of the x-ray picture or exhaustion caused by rigors workloads for the ordinary orthopaedist or even the expert orthopaedist might make it difficult to detect a fracture or fracture type using conventional procedures. This can be a challenge for orthopaedic professionals. The use of deep learning technology has the potential to reduce the severity of these unfavourable situations. In addition to having an accurate diagnosis, having a rapid diagnosis and reporting it is also very significant. The expedited approach will protect the patient from suffering injury as a result of a missing or delayed diagnosis [2] [3].

Images obtained from X-rays are commonly affected by Poisson noise, which not only lowers the overall visual quality of the picture but also obscures essential information that is necessary for making an accurate diagnosis [4]. Several researchers, among others, have used the incorporation of a denoising phase into the process of automated fracture identification. Since X-ray and CT scans, there are a variety of techniques that may be used to diagnose fractures. Wavelet and Curvelet, Haar, Support Vector Machine (SVM) classifier, X-Ray/CT auto classification of fracture (GLCM), Novel morphological gradient based edge detection technique, Daubechies Wavelet and Fuzzy C-Means (FCM) Clustering, Using Classifiers DT, BN, NB, NN, and mixed, Fusion Classification technique, Wavelet and Haar, Combined snake and GVF, and X-Ray/CT auto classification of fracture (GLCM) are some of the techniques that have been implemented [5]. An innovative method that makes use of binary trees and cutoffs, the use of the Discrete Wavelet Transform and the ring, the use of biplane slicing, the classification procedure based on supervised learning. Although there are a great number of retrospective studies about the automated assessment of bone fractures in humans, there are not a great number of studies that have been identified on animal fractures. Retrospective research has been conducted only with the purpose of determining the frequency of appendicular fractures in canines and felines [6].

Recent developments in digital image processing (DIP) methods provide interesting possibilities to overcome these difficulties [7]. It is now feasible to construct automated systems that can evaluate X-ray pictures with accuracy and dependability. This is made possible via the use of computational techniques and machine learning models. Not only can these devices speed up the diagnosis process, but they also provide vets with objective tools that enable them to make treatment choices based on accurate information [8].

This research was prompted by the junction of veterinary medicine and healthcare technology, which presented an opportunity for investigation [9]. Significant progress has been made in the field of veterinary diagnostics with the introduction of the capability to automatically identify fractures in X-ray pictures of animals. The purpose of this study is to bridge the gap between conventional diagnostic approaches and cutting-edge technology solutions by using potential of DIP techniques [10].

This major purpose is to create and assess an automated system for fracture diagnosis in animal X-ray pictures. This will be accomplished via the use of animals. Among the most important goals are:

- Making use of sophisticated feature extraction techniques, such as the Grey Level Co-occurrence Matrix (GLCM), to capture fine textural characteristics that are suggestive of fractures.
- Using Principal Component Analysis (PCA) to accomplish the reduction of the dimensionality of the retrieved features while maintaining the integrity of the pertinent information.

2. LITERATURE REVIEW

Older people, including both humans and animals are more likely to suffer from degenerative musculoskeletal disorders and injuries that have a substantial influence on their quality of life. It is well acknowledged that sarcopenia and osteoarthritis (OA) are the age-related musculoskeletal illnesses that are most frequent throughout the human population. Similarly, osteoarthritis (OA) is a primary cause of lameness in horses and it often results in chronic discomfort and death in older horses [11]. The incidence of osteoarthritis (OA) in aged people and horses is supported by parallels in pathophysiology, which has led to the extensive use of equine models for the purpose of studying pathological alterations connected to degenerative OA. There are also morphological and histological similarities between the human knee and tarsal joints and the horse tarsal joint [12]. This is in addition to the fact that osteoarthritis (OA) is a naturally occurring condition. There are notable parallels in the thickness and qualities of the articular cartilage in both situations, which makes it possible to successfully mimic the cellular structure and the biochemical consequences [13]. In addition, because of their bigger body size, horses provide an easier way to collect tissue and fluid samples, in addition to providing a diverse range of imaging modalities and clinical evaluation opportunities]. Taking into account all of these aspects, the relevance of monitoring osteoarthritis (OA) symptoms during treatment and rehabilitation in both human and veterinary applications is significantly diminished [14].

The primary objective of this work is to enhance diagnostic techniques for osteoarthritis of the tarsal joint in horses, which is generally known as bone spavin. The assessment of clinical symptoms, such as lameness and joint stiffness, is often the first step in the diagnostic process for equine osteoarthritis (OA) [15]. These symptoms frequently originate from the mild chronic inflammation that is associated with OA. As a result, the diagnostic procedure includes a fundamental clinical examination as well as an exhaustive orthopaedic evaluation, which is then completed with the use of flexion tests, local anaesthesia, and diagnostic imaging [16]. Various imaging modalities may be performed to examine the afflicted joint, including conven-tional radiography, ultrasonography, computed tomography (CT), magnetic resonance imaging (MRI), and, to a lesser degree, positron emission to-mography (PET). These methods are helpful in identifying structural abnormalities inside the clinically suspected joint. These changes include subchondral bone lysis or sclerosis, joint space alterations, and osteophyte development [17]. However, examinations of bone mineral density (BMD) and its link with the gradual loss of muscle mass, strength, and function are less routinely con- ducted. It is possible to carry out BMD assessment by using X-ray beam attenuation measurements, which may include single-energy X-ray computed digital absorptiometry (CDA) or dual-energy X-ray absorptiometry (DXA) [18]. Despite the fact that DXA is the technique of choice in human medicine [50–52], its applicability in clinical settings involving horses is restricted. When it comes to the first diagnostic imaging of bone spavin in horse treatment, traditional radiography is the predominant approach that is used [19]. The use of ultrasonography in the area of veterinary medicine is restricted owing to the fact that ultrasonic reflection occurs at the bone contact. This makes it difficult to evaluate the course of bone lesions. Imaging techniques such as computed tomography (CT), magnetic resonance imaging (MRI), and the most recent positron emission tomography (PET) need the transportation of the horse to specialised clinics, which may be costly and often require the horse to undergo general anaesthesia. The availability of these individuals for frequent field monitoring of the course of osteoarthritis is thus quite restricted [20].

3. METHODOLOGY

The proposed workflow is provided in Fig.1.

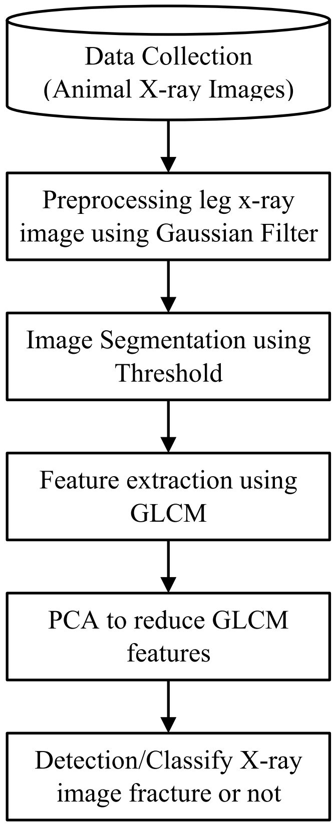

Fig.1. Block Diagram of Research Methodology

With a variety of digital image processing methods and machine learning algorithms, this research endeavour takes a methodical approach to the automation of fracture identification in animal X-ray pictures.

The dataset is comprised of X-ray images that were gathered from several prestigious veterinary institutions, such as the Karnataka Veterinary Animal and Fisheries Sciences University, the Veterinary Government Hospital Mahagaon, the Veterinary Government Hospital Kalaburagi, and the Veterinary College and Hospital Shivamogga. Additionally, Dr. Hegga, a veterinarian who practices in Kalaburagi, provided additional detailed descriptions.

3.1 DATA COLLECTION AND PREPROCESSING

The dataset that was obtained contains a variety of X-ray pictures of animals' legs. To provide high-quality inputs for further analysis, the pictures undergo preprocessing using a Gaussian filter, which smooths the images by minimising noise and highlighting essential aspect. This stage in the preprocessing process is very necessary in order to enhance the precision of the following picture segmentation and feature extraction procedures.

3.2 IMAGE SEGMENTATION

Image segmentation is carried out after the preprocessing stage to separate the bone structures from the tissues that are around them. The thresholding approaches that turn grayscale photos into binary images ensure that the bone structures are clearly differentiated from the background. This is accomplished by converting the grayscale images into binary images. For concentrating the study on pertinent anatomical characteristics that are symptomatic of fractures, the segmentation procedure is necessary.

3.3 FEATURE EXTRACTION

Following the segmentation of the bone structures, the Grey Level Co-occurrence Matrix (GLCM) is used in order to begin the process of feature extraction. The GLCM technique is a very effective way for analysing textures, since it involves quantifying the spatial correlations between the intensities of the pixels in the segmented pictures. It is possible that the existence of fractures may be inferred from the retrieved GLCM features since they capture key textural characteristics.

3.4 DIMENSIONALITY REDUCTION

Principal Component Analysis (PCA) is used in order to minimise the feature space while maintaining the most important information. This is done in light of the fact that the GLCM features have a high dimensionality. The Principal Component Analysis (PCA) method reduces the original characteristics to a more manageable number of uncorrelated components, which in turn simplifies the classification process and improves the efficiency of the calculation.

3.5 FRACTURE DETECTION AND CLASSIFICATION

After that, the reduced feature set that was created from principal component analysis is input into a machine learning classifier in order to detect whether or not fractures are present in the X-ray pictures. Using the retrieved characteristics, the classifier, which was trained on labelled datasets, is able to differentiate between pictures that have been fractured and those that have not occurred. This automated categorisation technique considerably improves diagnostic accuracy and consistency, so providing veterinarians with trustworthy instruments for the quick diagnosis of fractures.

For this reason, the technique incorporates data collecting, picture pre-processing, segmentation, feature extraction, dimensionality reduction, and classification based on machine learning in order to construct an automated fracture detection system. Not only does this technique make the diagnostic process more efficient, but it also contributes to the development of digital healthcare technology in the field of veterinary medicine.

3.6 DATA SET DESCRIPTION

Animal X-ray images were obtained from a number of authoritative veterinary institutions, including the Karnataka Veterinary Animal and Fisheries Sciences University in Bidar, the Veterinary Government Hospital in Mahagaon, the Veterinary Government Hospital in Kalaburagi, and the Veterinary College and Hospital in Shivamogga. These institutions were used to compile the dataset that was utilised in this study. Dr. Hegga, a veterinarian in Kalaburagi, contributed insightful annotations and thorough descriptions, which contributed to the enrichment of the information. Each picture was subjected to preprocessing, which included the use of a Gaussian filter for noise reduction, thresholding for segmentation, GLCM for feature extraction, and principal component analysis (PCA) for dimensionality reduction. The images were focused on leg areas that are prone to developing fractures. A robust automatic fracture diagnosis system that is accurate and adaptable across a variety of veterinary scenarios may be developed with the help of this diversified dataset that has been meticulously annotated.

3.7 PREPROCESSING BY USING GAUSSIAN FILTER

Within the realm of image processing, the Gaussian filter is a well-known technique that blurs or smoothes out pictures. In order to perform the function of a convolution filter, it makes use of a Gaussian kernel, which is a two-dimensional matrix of weights that is established by the Gaussian function. The main goal of filter is to make images appear visually smoother by suppressing fine details and reducing noise. Users can modify filter size and standard deviation, among other parameters, to regulate the degree of smoothing. Applications for the Gaussian filter include image smoothing, noise reduction, and computer vision pre-processing tasks.

The Gaussian is based on the Gaussian distribution, which is a continuous probability distribution function. The 1D Gaussian distribution function is given by:

$$G(x)=\frac{1}{\sqrt{2\pi\sigma}}e^{-\frac{x^2}{2\sigma^2}} \tag{1}$$

A high filter variance is useful in smoothing out noise when the Gaussian filter is employed for noise suppression; yet, at the same time, it distorts those regions of the picture where there are sudden changes in pixel brightness when it is being utilised. Additionally, the Gaussian filter is responsible for the shifting of edge positions, the disappearance of edges, and the appearance of phantom edges. There are two primary approaches that may be used to resolve these issues. The first technique involves pre-processing a picture by applying a variety of filters with varying filter variances and then identifying edges in the filtered images that have been produced. The end outcome of edge detection is a synthesis of the edge pictures made according to certain guidelines that have been pre-defined. The second technique involves adjusting the filter variance such that it corresponds to the local properties of a picture. The method that this is built on is that various regions of an image should be smoothed differently, depending on the degree of noise and the kind of edges that are present in the picture. It has been shown by Hodson and colleagues that the Gaussian filtering of a signal $F(x)$, which is represented $F_g(x)$, can be put into expression as:

$$F_g(x)=F(x)+\frac{F''(x)}{2}\sigma^2+\ldots+\frac{F^{(2m)}(x)}{\prod_{p=1}^{m}2p}\sigma^{2m}+.., \tag{2}$$

The second derivative of $F(x)$ is denoted by $F^{(2m)}(x)$, and the derivatives denoted by $F^{(2m)}(x)$ are the derivatives of $F(x)$ of the second order to the second order. It is possible to approximate the equation shown above by omitting the higher order.

$$F_g(x) = F(x) + \frac{F''(x)}{2}\sigma^2 \quad (3)$$

As a result, they explained the adaptive filter variance as follows:

$$\sigma^2(x) = \frac{2\grave{o}}{|F''(x)|} \quad (4)$$

where E is the amount of error that has been pre-defined as a result of Gaussian filtering. Using this approach, the error that is caused by filtering is roughly less than ϵ, i.e., $|F_g(x) - F(x)| \leq \grave{o}$. A For the purpose of estimating $F''(x)$ from the noisy corrupted signal, a sophisticated regression-based technique has been presented.

In order to solve the adaptive Gaussian filtering issue, a more sophisticated solution has been presented. This method treats the problem as the minimisation of the mean square error, with the restriction that the filter variance should not vary suddenly from pixel to pixel. If we designate the two-dimensional Gaussian filter as G and the image as F, respectively, then the optimum filter variance may be determined by minimising the expression E(σ) in the following equation:

$$E(\sigma) = \iint\left((F - G * F)^2 + \lambda\left|\nabla\sigma^{-1}\right|^2\right)dxdy \quad (5)$$

where "*" denotes convolution.

The Intensity-Dependent-Spread (IDS) model and the Contrast-Dependant Spread (CDS) filter are two examples of other adaptive Gaussian filters that have been presented in an effort to reflect the properties of the human visual system. The model known as the Intensity-Dependent-Spread model, which was suggested by Comsweet and Yellot, employs the inverse of the pixel brightness $F(x,y)$ (intensity) as the filter variance $\sigma(x,y)$.

$$\sigma(x,y) = 1/F(x,y) \quad (6)$$

Image improvement has been accomplished with the help of this model. Among the filters that Vaezi and Bavarian have investigated is the Contrast-Dependant Spread filter, which is often referred to as the composite-scale Gaussian filter. The filter variance in the CDS filter may be expressed as follows:

$$\sigma(x,y) = \frac{\sqrt{2}c}{\sqrt{2+c}} \quad (7)$$

where C is the contrast defined as: $C = \frac{|F(x,y) - F_a(x,y)|}{\max(F(x,y), F_a(x,y)}$

and $F_a(x,y)$ is the local mean brightness value.

Among the most important uses are:

- Image denoising is the process of making images less noisy at high frequencies while maintaining their edges.
- Improving the quality of a picture before proceeding with additional processing, such as edge detection or segmentation, is referred to as preprocessing.
- In the context of multi-scale image analysis, smoothing refers to the process of reducing the amount of detail present in images.

3.8 SEGMENTATION THE IMAGE (THRESHOLD)

To compute the statistical information of each and every pixel in a picture, a square-shaped operator, which might have a size of 3×3, 5×5, or 7×7 pixels, would be used. It's possible that a picture contains more than one thing. Following the operator's division of the picture into hundreds of blocks, the amount of information contained inside each block is significantly reduced. In this method, pixels with intensity values above a certain threshold are assigned one value (e.g., white), while those below the threshold are assigned another value (e.g., black).

When the threshold value is specified as 128. This means:

- Pixels with intensity values from 128 to 255 are set to white.
- Pixels with intensity values from 0 to 127 are set to black.

This technique is particularly useful for separating objects from the background in images where there is a clear distinction between the intensity values of the objects and the background.

Object and background are the only two grayscale zones that are presumed to be present in each block, according to the assumption. If the size of the structural operator is sufficiently modest, then the assumption is plausible, and the experiment will provide the confirmation that the assumption is correct. Within the scope of this study, the following approach is used to estimate the thresholds of the pixels that include an image: Let us assume that a picture is composed of just two primary grayscale areas, and let us use the symbol z to represent grayscale values. The histogram of these values may be regarded an approximation of their probability density function (PDF), which is denoted by the probability symbol p(z). These values are often believed to be random numbers. Specifically, this overall density function is the sum or combination of two densities, one of which represents the bright portions in the picture and the other of which represents the dark regions. An example of the mixing probability density function that describes the overall grayscale variation in the picture is as follows:

$$p(z) = P_1 p_1(z) + P_2 p_2(z) \quad (8)$$

That is, P_1 is the chance (a number) that a random pixel with value z is an object pixel. P_2 is the probability that the two classes of pixels will occur. Here, P_1 and P_2 are the probabilities of the occurrences of the two classes of pixels. The probability that the pixel in question is a background pixel is denoted by the symbol P_2. Any given pixel is presumed to belong to either an object or the backdrop, such that the situation may be described as follows:

$$P_1 + P_2 = 1 \quad (9)$$

The pixels in an image that have grayscale values that are larger than a threshold T are classified as background pixels, whereas the pixels that are not in this category are referred to as object pixels. The primary goal is to choose the value T that minimises the average mistake that occurs when determining whether a particular pixel belongs to an item or to the background since this is the most important aim. Both the PDF of the object and the backdrop are denoted by the letters $P_1(z)$ and $P_2(z)$, respectively. The likelihood of incorrectly identifying a backdrop point as an object point is equal to the chance that is

$$E_1(T) = \int_{-\infty}^{T} p_2(Z)\,dz \quad (10)$$

In a similar, the probability of incorrectly identifying a point on an item as a backdrop point is

$$E_2(T)=\int_T^{\infty} p_1(Z)\,dz \tag{11}$$

Then the overall probability of error is

$$E(T)=P_2E_1(T)+P_1E_2(T) \tag{12}$$

To find the threshold value for which the error $E(T)$ is minimal that requires differentiating $E(T)$ with respect to T (using Leibniz's rule) and equating the result to 0. The result is

$$P_1p_1(T)=P_2p_2(T) \tag{13}$$

In order to get an analytical expression for T, it is necessary to be familiar with the equations for both of the PDFs. It is not always possible to estimate these densities in practice; hence, one method that is often used is to make use of densities whose parameters are relatively easy to get with reasonable ease. According to this method, the Gaussian density is one of the most important densities that is used. In this particular instance,

$$p(Z)=\frac{p_1}{\sqrt{2\pi}\sigma_1}e^{-\frac{(z-\mu_1)^2}{2(\sigma_1)^2}}+\frac{p_2}{\sqrt{2\pi}\sigma_2}e^{-\frac{(z-\mu_2)^2}{2(\sigma_2)^2}} \tag{14}$$

Where μ_1 and $(\sigma_1)^2$ are the mean and variance of the Gaussian density of the object pixels, and μ_2 and $(\sigma_2)^2$ are the mean and variance of the Gaussian density of the background pixels. Substituting the below eqn then we can get the following quadratic equation and also the solution of threshold T,

$$AT^2+BT+C=0 \tag{15}$$

The analysis described above may also be found in the individual blocks that make up a picture. In this particular study, it is possible to estimate the threshold of a pixel by calculating the mean of the grayscale values of its neighbouring pixels. This is in contrast to the traditional method of calculating the mean of μ_1 and μ_2.

$$T_{ij}=\frac{1}{(2m+1)(2n+1)}\sum_{x=-m}^{m}\sum_{y=-n}^{n}z(i+x,\,j+y) \tag{16}$$

That is, the grayscale value of the pixel that is placed in (i,j) is denoted by the expression $z(i,j)$. Also, m and n are also examples of natural numbers. It is presumed that the pixel belongs to the object if the value of $z(i,j)$ is smaller than T_{ij}; otherwise, it is assumed that the pixel belongs to the background. In point of fact, even if there is a little variation in the estimate of the threshold T_{ij}, the outcome of the segmentation algorithm would not be significantly altered. In addition, the experiment will provide the evidence. The variance of the grayscale values of the pixels in a block that includes both the object and the background at the same time is unquestionably higher than the variance of a block that contains just the object or only the background. This is the case when there is a block in an image that contains both the object and the backdrop at the same time. When the variation in grayscale values of pixels inside a block is taken into consideration, as shown in the following illustration, it is possible to get the edge within this block.

$$\sigma_{ij}{}^2=\frac{1}{(2m+1)(2n+1)}\sum_{x=-m}^{m}\sum_{y=-n}^{n}z(i+x,\,j+y)-T_{ij}{}^2 \tag{17}$$

If the grayscale value of a pixel is lower than its threshold and the variance of the grayscale values of the pixels in its neighbours is higher than the given value Delta, then this pixel is defined as the boundary, and its grayscale value is evaluated as 0. If either of these conditions is not met, then the pixel is defined as the background, and its grayscale value is evaluated as 255. According to the suggested technique, the variance of the grayscale values of the pixels in this block may be replaced by the grayscale value difference between the brightest pixel and the darkest pixel in this block. This will result in a reduction in the complexity of the algorithm.

3.9 AFTER SEGMENTATION GROUND TRUTH COMPARE

After segmentation, the segmented image is compared to the ground truth to evaluate the performance of the algorithm. This comparison can be done using metrics such as accuracy, precision, recall, and the F1-score to quantify how well the segmentation matches the ground truth labels.

Algorithm

1. **Calculate Local Threshold**: Compute $T_{i,j}$ for each pixel (i,j).
2. **Classify Pixels**: Determine if each pixel belongs to the object or background based on $T_{i,j}$.
3. **Compute Variance**: Calculate $\sigma_{ij}{}^2$ for each pixel's neighborhood.
4. **Detect Boundaries**: Classify boundary pixels based on grayscale value and variance.
5. **Simplify Variance Calculation**: Optionally use the difference between the brightest and darkest pixels to approximate variance.
6. **Compare to Ground Truth**: Evaluate segmentation results against ground truth using standard metrics.

This approach allows for effective image segmentation by leveraging local statistics and adaptive thresholding, which can handle variations in lighting and object texture within the image.

3.10 FEATURE EXTRACTION (GLCM)

The piece of information that is vital for solving a particular application and for representing key qualities of pictures is often referred to as features. One of the most important factors that determines the accuracy of classification and the needs for training sets is the selection of input characteristics. The technique of collecting the visual contents of photographs is known as feature extraction. The objective of this procedure is to reduce the amount of resources that are typically needed. A grey level co-occurrence matrix, often known as GLCM, was developed as part of this research project in order to extract statistical texture properties. Texture characteristics are essential low-level features that are utilised to characterise the contents of an image, such as quantifying the texture that is perceived in an image. The method is well-known for its ability to extract second-order statistical texture characteristics by making use of statistical distributions of intensity value combinations at various places in relation to one another inside an image. Statistics may be broken down into three different orders: first, second, and higher order, dependant on the amount of intensity points present in a picture. Although higher levels of statistics are theoretically feasible, they are not viable to execute owing to the complexity of the computations involved. Information on the structural arrangement of surfaces and their relationships with the surrounding environment is included within the qualities of texture. It is possible to acquire a total of twenty-two texture-based characteristics, which include energy, correlation, entropy, inverse difference moment (IDM), homogeneity, sum variance, autocorrelation, contrast, maximum probability, dissimilarity, and IDM normalised, amongst many more. Only a handful of them are comprised of the following:

Energy: There are a few other names for energy, including “uniformity” and “angular second moment.” The sum of square components in the GLCM matrix is represented by this. It does this by comparing areas that are homogenous to those that are not homogeneous. When the frequency of repeated picture pixels is high, it is said to be high.

$$Energy = \sum_{i,j=0}^{N-1} (P_{ij})^2 \tag{18}$$

Entropy: The unpredictability of the picture is determined by this function. As a consequence of this, a homogenous picture will produce entropy values that are lower.

$$Entropy = \sum_{i,j=0}^{N-1} -ln(P_{ij})P_{ij} \tag{19}$$

Contrast: It provides a measurement of the strength of the contrast that exists between a pixel and its neighbour over the whole picture.

$$Contrast = \sum_{i,j=0}^{N-1} P_{ij}(i-j) \tag{20}$$

Correlation: It is a measurement of the linear relationships there are between grey tones in a picture. Specifically, it describes the manner in which a pixel is connected to its neighbour.

$$Correlation = \sum_{i,j=0}^{N-1} P_{ij} \frac{(i-\mu)(j-\mu)}{\sigma^2} \tag{21}$$

Homogeneity: The degree of similarity between pixels is described. When applied to a homogeneous picture, the GLCM matrix yields a value of 1. In the event that the picture texture needs just minor adjustments, it is very low.

$$Homogenity = \sum_{i,j=0}^{N-1} \frac{P_{ij}}{1+\left(i-j\right)} \tag{22}$$

where, P_{ij}= $(i,j)^{th}$ element of normalized GLCM matrix.

3.11 PCA FOR REDUCED FEATURES

A big number of features may raise computation time and complexity problems, waste a considerable amount of storage memory, and occasionally make categorisation more challenging. This phenomenon is referred to as the “dimensionality curse.” PCA, for example, has the ability to reduce the number of principle components to a more manageable size if we begin with twenty features that have been collected using GLCM. Using principal component analysis, the initial twenty characteristics are reduced to five principle components in this example. During this reduction procedure, the bulk of the variation that was there in the initial data is preserved. This ensures that the information that is most relevant is kept while simultaneously removing noise and redundancy. Despite the fact that features are essential for obtaining high accuracy, the issue persists when there are a large number of features. In addition, an increased number of characteristics resulted in an issue known as “overfitting,” which caused the system to lose its generality, which in turn led to low accuracy. Therefore, it is necessary to design approaches that pick the “optimal subset of features” from a wider collection of features. These approaches are referred to as feature selection strategies. All of the information that is provided in the original set is also included in the reduced set. In order to accomplish the goal of feature reduction, this work incorporates principal component analysis (PCA). It is a well-known dimensionality reduction approach that lowers a big number of correlated variables to a smaller set of uncorrelated variables known as principle components. This reduction process maintains the majority of the variations that were present in the original data. Another way to think about it is as the rotation of the axes of the original variables to a new set of orthogonal axes, which are known as the primary axes. This is done in such a way that the new coordinate system includes the direction of the largest fluctuations of the original variables. Multiple uses of principal component analysis include face recognition, picture compression, gene expression research, and a great deal more. The first primary axis has the biggest number of data variations that are conceivable, the subsequent component contains the greatest number of variations that are still available, and so on. The PCA begins with normalisation as a precondition. In order to have the principal component analysis (PCA) implemented in Python, the initial vector has to be normalised (that is, within the range of -1 to 1) or zero-centered (z-score).

The following impacts on data are caused by the adoption of PCA:

- By orthogonalizing the original vectors, principal component analysis (PCA) ensures that the resulting vectors are not connected with one another.
- It ranks the components that were produced in such a way that the component that has the highest variance is placed at the top of the list; also, it removes the vectors that have the least amount of variation in the data set.

By using principal component analysis (PCA), the purpose of this study is to strike a balance between the efficiency of computing and the accuracy of classification. This will ensure that the information that is most pertinent is kept while simultaneously removing noise and redundancy.

4. EXPERIMENTAL RESULTS

In this study, we employed GLCM and connected regions for feature extraction from MRI images. The experiment involved two types of MRI scans: one depicting a benign tumor and another representing a normal MRI without any tumor presence. Feature Extraction and Analysis: GLCM Texture Features: We computed texture features from the GLCM to characterize the grayscale patterns within each MRI. These features provided insights into the texture variations associated with different tumor grades and the absence of tumors. Connected Regions for Shape Features: Utilizing connected regions, we extracted shape features such as circularity, area, and perimeter from segmented MRI images.

These features helped quantify the geometric properties of tumors and normal brain tissues.

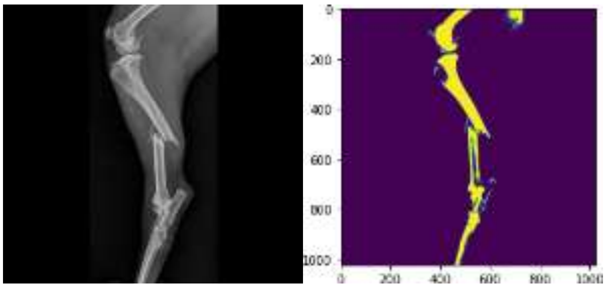

Fig.2. Data 1 (original vs classified image)

For the Figure, the GLCM features extracted from the image, the mean GLCM value was found to be very low (1.53e-05), indicating subtle variations in texture. The standard deviation of GLCM values was 0.00306, suggesting moderate variability in texture patterns across the image. The maximum GLCM value observed was 0.784, indicating areas of pronounced texture co-occurrence. These findings collectively led to the detection of a fracture in the analyzed image, highlighting the effectiveness of GLCM-based image processing techniques in identifying structural abnormalities.

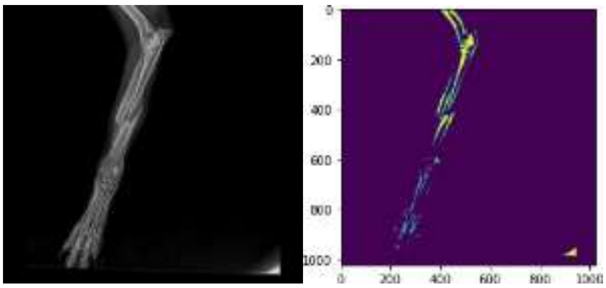

Fig.3. Data 2 (original vs classified image)

The mean GLCM value of 1.53e-05 indicates low overall texture complexity, while the standard deviation of 0.00306 suggests moderate variability in texture patterns. The maximum GLCM value observed was 0.784, indicating areas with significant texture co-occurrence. These findings led to the detection of a fracture in the analyzed image."

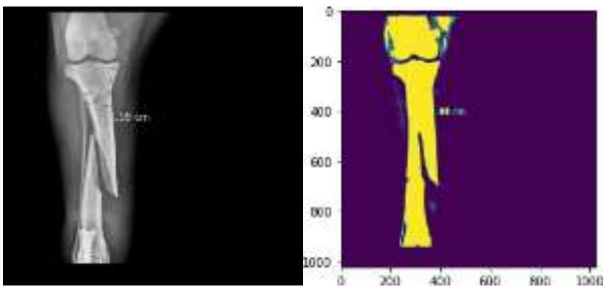

Fig.4. Data 3 (original vs classified image)

The mean GLCM value of approximately 1.53e-05 indicates very low texture complexity across the image. The standard deviation of GLCM values, at 0.00287, reflects relatively uniform texture patterns with slight variability. The maximum GLCM value observed was 0.736, suggesting localized areas of pronounced texture co-occurrence. These findings collectively supported the detection of a fracture in the image, underscoring the efficacy of GLCM-based analysis in identifying structural abnormalities."

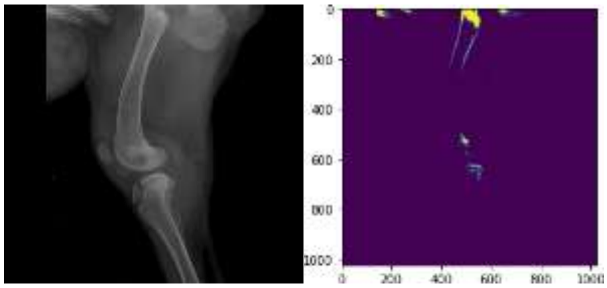

Fig.5. Data 4 (original vs classified image)

The mean GLCM value of approximately 1.53e-05 suggests very low texture complexity throughout the image. The standard deviation of GLCM values, measured at 0.00225, indicates minimal variability in texture patterns across the analyzed area. The maximum GLCM value observed was 0.576, indicating areas with moderate texture co-occurrence. These findings collectively indicate no fracture detected in the image, highlighting the consistent texture patterns observed.

Table.1. Experimental Data

Figure	Mean GLCM	SID GLCM	Max GLCM	Classification
1	1.525×10^{-5}	0.0020	0.590	Fracture detected in image
2	1.525×10^{-5}	0.0030	0.784	Fracture detected in image
3	1.525×10^{-5}	0.0028	0.736	Fracture detected in image
4	1.525×10^{-5}	0.0022	0.576	No fracture detected in image

5. CONCLUSION

A technique for adaptive picture segmentation that makes use of local thresholding and variance analysis is presented in this scientific study. The approach is able to accommodate differences in illumination and texture since it calculates local thresholds based on the mean grayscale values of nearby pixels. The use of variance analysis helps to further enhance boundary detection, which in turn ensures that edge pixels are classified accurately. The computational cost of the technique is reduced by the use of a simplified variance calculation, which makes the approach acceptable for use in real-time applications. The results of the experiments demonstrate the accuracy and resilience of the approach, indicating that it achieves the desired outcomes in a variety of imaging situations. For the purpose of improving segmentation, it is possible that future study may concentrate on optimising the algorithm for pictures that are more complex and adding extra contextual information.

REFERENCES

[1] B. Baydan and H.M. Unver, "Detection of Tibial Fractures in Cats and Dogs with Deep Learning", *Ankara Universitesi Veteriner Fakültesi Dergisi*, Vol. 68, No. 3, pp. 283-290, 2021.

[2] G.B. Ergun and S. Guney, "Classification of Canine Maturity and Bone Fracture Time based on X-Ray Images of Long Bones", *IEEE Access*, Vol. 9, pp. 109004-109011, 2021.

[3] K.C. Santos, C.A. Fernandes and J.R. Costa, "Feasibility of Bone Fracture Detection using Microwave Imaging", *IEEE Open Journal of Antennas and Propagation*, Vol. 3, pp. 836-847, 2022.

[4] B. Baydan, N. Barisci and H.M. Unver, "Determining the Location of Tibial Fracture of Dog and Cat using Hybridized Mask R-CNN Architecture", *Kafkas Universitesi Veteriner Fakultesi Dergisi*, Vol. 27, No. 3, pp. 1-15, 2021.

[5] G.B. Ergun and S. Guney, "Image Data Augmentation Techniques for Fracture Detection of Dogs", *Proceedings of International Conference on Engineering Science and Technology*, pp. 214-224, 2021.

[6] G.B. Cangoz and S. Guney, "The Effects of the Traditional Data Augmentation Techniques on Long Bone Fracture Detection", *Bilge International Journal of Science and Technology Research*, Vol. 7, No. 1, pp. 63-69, 2023.

[7] K.C. Santos, C.A. Fernandes and J.R. Costa, "Experimental Evaluation of Thin Bone Fracture Detection using Microwave Imaging", *Proceedings of European Conference on Antennas and Propagation*, pp. 1-3, 2022.

[8] S.J.A. Ibrahim, and N.K. Chakravarthy, "Deep Learning-Driven Prediction Model for Antiviral–HPV Protein Interactions Using Amino Acid Sequence Frequency Encoding", *Proceedings of International Conference on Sustainable Developments in Computer Engineering, Green Technology and Smart Systems*, pp. 472-477, 2026.

[9] G. Moon, S. Kim, W. Kim, Y. Kim, Y. Jeong and H.S. Choi, "Computer Aided Facial Bone Fracture Diagnosis (CA-FBFD) System based on Object Detection Model", *IEEE Access*, Vol. 10, pp. 79061-79070, 2022.

[10] Y.S. Chen, S.D. Luo and W.C. Lin, "Improving Detection of Impacted Animal Bones on Lateral Neck Radiograph using a Deep Learning Artificial Intelligence Algorithm", *Insights into Imaging*, Vol. 14, No. 1, pp. 21-43, 2023.

[11] P. Augat, E.F. Morgan, T.J. Lujan and W.H. Cheung, "Imaging Techniques for the Assessment of Fracture Repair", *Injury*, Vol. 45, pp.16-22, 2014.

[12] C. Lu, R. Marcucio and T. Miclau, "Assessing Angiogenesis during Fracture Healing", *The Iowa Orthopaedic Journal*, Vol. 26, pp. 1-17, 2006.

[13] S.A. Jones, M.B. Whitcomb, B. Vaughan, B. Busch and M. Spriet, "Ultrasonographic Diagnosis of Femoral Fractures in Large Animals", *Journal of the American Veterinary Medical Association*, Vol. 260, No. 13, pp. 1675-1682, 2022.

[14] C. Rufener, S. Baur, A. Stratmann and M.J. Toscano, "A Reliable Method to Assess Keel Bone Fractures in Laying Hens from Radiographs using a Tagged Visual Analogue Scale", *Frontiers in Veterinary Science*, Vol. 5, pp. 124-132, 2018.

[15] T. Wang, H. Wang, K. Wang and Z. Yang, "Research on Image Mosaic Method based on Fracture Edge Contour of Bone Tag", *Applied Sciences*, Vol. 13, No. 2, pp. 756-766, 2023.

[16] R.K. Sharma, S. Mishra, M. Sharma and A.K. Bishnoi, "Management of Long Bone Fractures using Diverse Fracture Fixation Techniques in Small Animals", *Journal of Scientific Research and Reports*, pp. 107-120, 2022.

[17] K. Yezzi Woodley, A. Terwilliger, J. Li, E. Chen and P. Olver, "Using Machine learning on New Feature Sets Extracted from Three-Dimensional Models of Broken Animal Bones to Classify Fragments according to Break Agent", *Journal of Human Evolution*, Vol. 187, pp. 103495-103513, 2024.

[18] Z. Liu, F. Liu and Y. Yang, "Estimation of Drinking Water Volume of Laboratory Animals based on Image Processing", *Scientific Reports*, Vol. 13, No. 1, pp. 8602-8615, 2023.

[19] A.M. Knox, A.C. McGuire, R.M. Natoli and C.D. Collier, "Methodology, Selection, and Integration of Fracture Healing Assessments in Mice", *Journal of Orthopaedic Research*, Vol. 39, No. 11, pp. 2295-2309, 2021.

[20] L. Jin, J. Yang, K. Kuang and M. Li, "Deep-Learning-Assisted Detection and Segmentation of Rib Fractures from CT Scans: Development and Validation of FracNet", *EBioMedicine*, Vol. 62, pp. 1-15, 2020.